



In situ fabrication of Bi₂O₂CO₃/MoS₂ on carbon nanofibers for efficient photocatalytic removal of NO under visible-light irradiation

Jundie Hu, Dongyun Chen*, Najun Li, Qingfeng Xu, Hua Li, Jinghui He, Jianmei Lu*

College of Chemistry, Chemical Engineering and Materials Science, Collaborative Innovation Center of Suzhou Nano Science and Technology, Soochow University, Suzhou, 215123, China

ARTICLE INFO

Article history:

Received 23 February 2017

Received in revised form 24 April 2017

Accepted 30 May 2017

Available online 3 June 2017

Keywords:

Novel photocatalyst

NO removal

Visible-light irradiation

Recyclable

ABSTRACT

A novel nanocomposite photocatalyst for NO removal, Bi₂O₂CO₃-MoS₂-CNFs, was fabricated by an efficient method. This new photocatalyst performed impressively in the removal of NO at low concentration (600 ppb), with a maximum efficiency of 68% under visible-light irradiation, superior to most other visible-light photocatalysts. Its high performance was ascribed to the introduction of carbon nanofibers as carriers, and MoS₂, which enhanced the absorption of visible light and accelerated the separation and transfer of electrons and holes. Photocurrent tests and electrochemical impedance spectroscopy also demonstrated that Bi₂O₂CO₃-MoS₂-CNFs had a high efficiency of interfacial charge separation, which is critical to improving the photocatalytic activity. Moreover, the membrane of the photocatalyst was stable and recyclable after multiple runs. All of these factors demonstrate its potential application in the removal of NO from air.

© 2017 Published by Elsevier B.V.

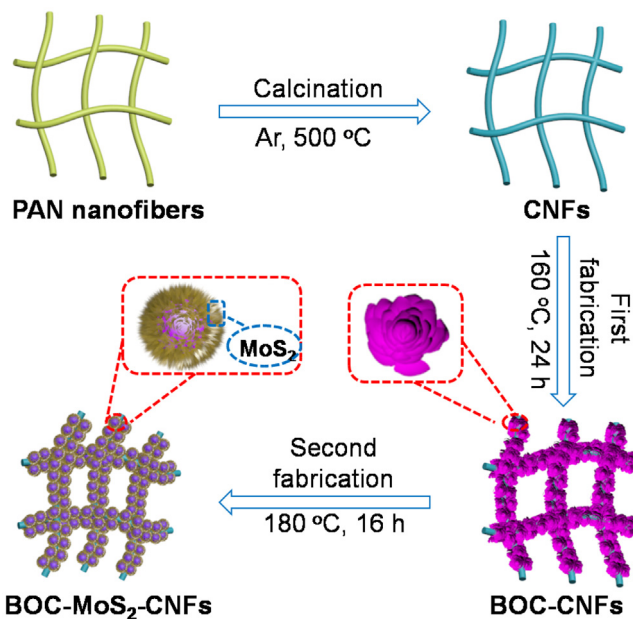
1. Introduction

With the rapid economic and industrial development of China, the number of automobiles in the country is increasing. The growing discharge of automobile exhaust gases into the air is a major cause of environmental pollution. Consequently, the concentration level of PM 2.5 (PM \leq 2.5 μm in aerodynamic diameter, PM is particulate matter) in major cities is well above the National Ambient Air Quality Standard [1,2]. Recently, China has experienced severe haze events caused by secondary aerosol precursors [3,4]. Nitrogen oxides (NO_x, mainly comprising NO and NO₂) are important contributors to these pollution incidents. Therefore, the development of efficient and economical technologies to address the NO pollution problem is an urgent matter. There are many established techniques and methods for NO purification under ambient conditions, for example physical adsorption [5–7], biofiltration [8–10], thermal catalytic reduction [11,12] and selected catalytic reduction [13–15], but these methods are uneconomical and inefficient for the removal of NO at the parts per billion (ppb) level. However, semiconductor photocatalysis [16,17] is considered a promising technology for NO removal at ppb levels, with potential value in addressing the worldwide energy shortage, because of its high efficiency and eco-friendly characteristics.

Research into photocatalysts for NO removal initially focused on TiO₂ because of its low cost, non-toxicity and high activity, but TiO₂ can only be activated by UV light ($\lambda < 400 \text{ nm}$), which limits its practical application [18–26]. In subsequent research, several novel photocatalysts, including *g*-C₃N₄-based materials [27–31], Bi-based materials [32–38], hematite (Fe₂O₃) [39] and Mn⁴⁺-doped anatase [40], have been investigated, and exhibited high performance in the removal of NO at low concentration. Among these, the Bi₂O₂CO₃ photocatalyst [32–35] has attracted particular attention because of its promising applications as a supercapacitor, low mammalian toxicity and good photocatalytic ability. Pure Bi₂O₂CO₃ nanoparticles were shown to remove NO with a percentage removal of 25% [41], while hierarchical Bi₂O₂CO₃ structures achieved a removal of 46% [42], illustrating that the morphology of the photocatalyst plays a significant role in its catalytic effectiveness. However, acceptable results cannot be achieved with the use of a single semiconductor. Therefore, a series of strategies have been developed to improve the photocatalytic efficiency of Bi₂O₂CO₃, including element doping [43], surface modification [44] and the construction of heterojunctions [32,35]. Compared with single semiconductors, heterojunctions inhibit the recombination of photoinduced electron–hole ($e^- - h^+$) pairs and contribute to electron transport, thereby improving the photocatalytic efficiency. Lee and coworkers fabricated a Bi₂O₂CO₃/*g*-C₃N₄ heterojunction for photocatalytic NO removal, and the NO removal ratio of this heterojunction was 29.4% higher than that of pure Bi₂O₂CO₃ [35]. Zang and coworkers constructed a three-dimensional Z-scheme

* Corresponding authors.

E-mail addresses: dychen@suda.edu.cn (D. Chen), lujm@suda.edu.cn (J. Lu).



Scheme 1. Schematic illustration of the fabrication of BOC-MoS₂-CNFs.

(BiO)₂CO₃/MoS₂, which dramatically enhanced the photocatalytic NO removal by a factor of 2.2 times compared with pure Bi₂O₂CO₃ under visible light [32], because of the fast separation and transfer of e⁻ and h⁺ enabled by the introduction of MoS₂. However, powder photocatalysts are difficult to recycle because they can be easily blown away during use. Thus, it is important to immobilize the photocatalyst on a suitable carrier.

In this work, Bi₂O₂CO₃-MoS₂-CNFs nanocomposites were fabricated and successfully used to remove NO at the ppb level under visible-light irradiation. Carbon nanofibers (CNFs) were obtained by the calcinations of PAN (polyacrylonitrile) nanofibers [45,46]. Rose-like Bi₂O₂CO₃ microflowers were modified on the surface of the CNFs, and then wrapped by thin MoS₂ nanosheets, as shown in **Scheme 1**. Here, the CNFs not only acted as a carrier to bind the powder photocatalyst, thus facilitating the transportation of e⁻, but also played the role of an adsorbent for NO. The experimental results showed that the Bi₂O₂CO₃-MoS₂-CNFs photocatalyst achieved an NO removal ratio of 68%, which is superior to most other visible-light photocatalysts. Therefore, the Bi₂O₂CO₃-MoS₂-CNFs membranes have a potential application value in the removal of NO from air in the future.

2. Experimental

2.1. Materials

Polyacrylonitrile (PAN, MW = 150,000), bismuth citrate, sodium molybdate (Na₂MoO₄) were purchased from Sigma Aldrich. Sodium carbonate (Na₂CO₃) were purchased from Adamas. N,N-dimethylformamide (DMF), thioacetamide (TAA) and ethylene glycol were purchased from Sinopharm Chemical ReagentCo., Ltd (China) and deionized water was used throughout the experiments. All the chemicals were used without further purification.

2.2. Synthesis of CNFs

In a typical process, CNFs were prepared using an electrospinning machine. 1.0 g of PAN was dissolved into 9.0 mL of DMF in a 20 mL reaction flask, then the mixture under magnetic stirring at room temperature for about 12 h. The above clarified solution

was placed in a 5 mL syringe with a flattened metal needle. The electrospinning was carried out at a positive voltage of 15 kV and negative voltage of -5 kV, the dosing speed was 0.2 mm min⁻¹ and then the PAN nanofibers were obtained. Subsequently, the white polymer nanofibers were heated from room temperature to 500 °C under flowing Ar for 4 h with a ramp rate of 2 °C min⁻¹, then black products were obtained.

2.3. Preparation of Bi₂O₂CO₃-CNFs

Bi₂O₂CO₃-CNFs were prepared by a simple hydrothermal method [32] according to previously described process with some modifications as follows: 230 mg Na₂CO₃ was dissolved in a mixed solution of deionized water (30 mL) and ethylene glycol (6 mL) and stirred for 30 min, then 800 mg bismuth citrate was added into the above suspension and stirred for another 30 min, transparent solution was obtained. Subsequently, the precursor suspension and 50 mg CNFs were transferred into a 50 mL Teflon-lined stainless autoclave and heated at 160 °C for 24 h. After reaction, the reacted mixture was collected with a tweezers and washed with deionized water and ethanol for three times respectively, then dried in an vacuum oven at 60 °C for 6 h. The product Bi₂O₂CO₃-CNFs was obtained and labeled as BOC-CNFs. The pure Bi₂O₂CO₃ microflowers were synthesized under the same conditions without adding CNFs, and labeled as BOC.

2.4. Preparation of Bi₂O₂CO₃-MoS₂-CNFs

Firstly, 24.2 mg Na₂MoO₄ and 19.4 mg thioacetamide were dissolved in 30 mL of deionized water and ultrasound for 30 min, then the mixture and the above BOC-CNFs were transferred to a 50 mL Teflon-lined stainless autoclave and heated at 200 °C for 16 h. Finally, the product was collected and washed with deionized water and ethanol for three times respectively, then dried in an vacuum oven at 60 °C for 6 h. The obtained product Bi₂O₂CO₃-MoS₂-CNFs was labeled as BOC-MoS₂-CNFs. The pure MoS₂ was synthesized under the same conditions without adding BOC-CNFs [47].

2.5. Characterization

Scanning electron microscopy (SEM) (Hitachi S-4800) coupled with X-ray energy dispersive spectroscopy (EDS), and transmission electron microscopy (TEM) (Hitachi H600, 200 kV) were used to measure the morphology, element and crystal lattice of the samples. X-ray diffraction (XRD) (X'Pert-Pro MPD) was used to investigated the crystallographic structure of the products. X-ray photoelectron spectroscopy (XPS) analysis was performed in an X-ray photoelectron spectrometer (ESCALAB MK II) using Al-K α radiation as the exciting source. Using the UV-vis spectrophotometer (CARY50) and fourier transform infrared (FTIR) spectrometer (Nicolet 4700) to measure the light absorbance spectra of samples. The photoluminescence (PL) spectra of the samples were recorded by using a fluorescence spectrophotometer (FLS920) with an excitation wavelength of 370 nm. Electron spin resonance (ESR) spectra of paramagnetic species spin-trapped with 5,5-dimethyl-L-pyrroline-N-oxide (DMPO) were recorded with a Bruker A300 EPR spectrometer. Electrochemical measurements were conducted with a CHI 660 B electrochemical system (Shanghai, China) with a standard three-electrode cell, Pt plate was used as the counter electrode and Ag/AgCl electrode was used as the reference electrode, the samples were made as the working electrode, Na₂SO₄ (0.1 M) was used as the electrode solution. 10 mg sample was ground into powder and dispersed in 10 mL of deionized water by sonication to get a slurry. The slurry was spread onto surface of indium-tin oxide (ITO) glass, the working electrode was obtained after the ITO glass was dried at 393 K for 3 h. Visible-light irradiation was provided

by Xenon lamp (300W, simulated sunlight). The electrochemical impedance spectra (ESI) measurements were also performed on this electrochemical workstation [48–50].

2.6. Evaluation of photocatalytic activity

The photocatalytic activities of the as-prepared samples were investigated in terms of the photocatalytic removal of NO at ppb levels, which was performed in a continuous flow reactor at ambient temperature under visible light irradiation. The volume of the cylindrical reactor made of glass was 1.6 L (Φ 10 × 20 cm) and 0.15 g of catalyst was placed in the center of it. The Xenon lamp was vertically placed outside the reactor above the reactor. NO gas was supplied by a compressed gas cylinder at a concentration of 100 ppm of NO (N₂ balance). The initial concentration of NO was diluted to about 600 ppb via air stream provided by a compressed air cylinder. The two gas streams were premixed in a three-way valve and the flow rate of the mixed gas was controlled at 2.4 L min⁻¹. The desired humidity level of the air flow was controlled at 50% by passing the air stream through a humidification chamber. When the adsorption-desorption equilibrium among photocatalyst, gas and water vapor was achieved in half an hour, the Xenon lamp was turned on. The concentration of NO was consequently measured every one minute by using a NO_x analyzer (Thermo Environmental Instruments, Inc., 42i-TL), which also monitored the concentration of NO₂. The removal efficiency η (%) of NO was calculated as: η (%) = $(1 - C/C_0) \times 100\%$, where C and C_0 were the concentrations of NO in the outlet stream and the feeding stream respectively.

3. Results and discussion

3.1. Morphology and structure

The morphology and structure of the CNFs, BOC-CNFs and BOC-MoS₂-CNFs were analyzed by SEM and TEM. As displayed in Fig. S1 (Supporting Information), the SEM images of the PAN nanofibers and CNFs demonstrated that the surfaces were smooth with a large surface area, providing favorable conditions for the modification of the photocatalyst. Interestingly, BOC grew on the CNFs in the form of rose-like microflowers, with branches tightly wrapped in large numbers of roses, as shown in the SEM images in Fig. 1a and b. All the microflowers were of the same size and connected together tightly. Fig. 1c and d show the low-magnification and high-magnification SEM images, respectively, of the BOC-MoS₂-CNFs. In contrast to BOC, MoS₂ nanoflakes grew on the surface of the BOC-CNFs in a uniform shape resembling ice-sugar gourds. Fig. 1d clearly shows that the MoS₂ nanoflakes were considerably thinner than the BOC-CNFs. For comparison, Fig. S2a and S2b (Supporting Information) show SEM images of pure BOC microflowers and MoS₂, respectively. TEM images of the BOC-MoS₂-CNFs are presented in Fig. 1e and 1f. These confirm the presence of rose-like BOC microflowers attached to the CNFs and wrapped in MoS₂ flakes. From the HRTEM images (Fig. 1g and 1h, high-magnification images of the yellow and blue circles, respectively, in Fig. 1f), the lattice fringes of a single BOC nanoflake can be estimated as 0.271 nm, which is consistent with the spacing of its (110) crystal facet [33–35]. Meanwhile, the (002) plane of MoS₂ (with a lattice spacing of 0.62 nm) [47] can also be observed clearly. From these SEM and TEM images, it can be deduced that the interfacial interaction between MoS₂ and BOC would enable fast electron transfer during irradiation by visible light.

Energy dispersive spectroscopy (EDS) mapping images are shown in Fig. 2, and reveal that the elements Bi, C, O, Mo and S were uniformly deposited on the surface of the CNFs, as illustrated by the

color intensities. Additionally, SEM-EDS analysis of the BOC-MoS₂-CNFs (Fig. S3, Supporting Information) verified the above structural descriptions and elemental contents.

3.2. Phase and composition

The crystalline structures of the obtained samples were characterized by powder X-ray diffraction. The XRD patterns of the as-prepared samples are shown in Fig. 3a and b. All the diffraction peaks of BOC can be perfectly indexed to pure tetragonal BOC (JCPDS no. 41–1488), with no other diffraction peaks being detected, demonstrating the existence and purity of BOC. No changes of the diffraction peaks of BOC were detected in the BOC-CNFs and BOC-MoS₂-CNFs samples, which implied that BOC grew on the surface of the CNFs without any chemical reaction. However, the (013) ($2\theta = 30.2^\circ$) and (110) ($2\theta = 32.7^\circ$) peaks of BOC [32] weakened in intensity following loading onto the CNFs, indicating a slight reduction in the crystallinity of BOC, as shown in Fig. 3b. The major diffraction peaks of MoS₂ can be clearly seen in the XRD pattern of the BOC-MoS₂-CNFs. The peaks at 13.8° and 33.1° were attributed to the (002) and (100) planes of MoS₂, respectively [47]. The (110) peak of MoS₂ could not be observed in this sample because of overlapping between the diffraction peak of BOC and the (110) peak of MoS₂ at 58.5° . In summary, we concluded that the MoS₂ nanoflakes had been successfully modified on the surface of the BOC-CNFs.

The chemical nature and surface composition of the BOC-MoS₂-CNFs sample were further investigated by XPS, as shown in Fig. 4. The XPS survey spectrum showed the expected O, C, Bi, Mo and S elements in the BOC-MoS₂-CNFs (Fig. 4a), and high-resolution XPS spectra were recorded for all of these elements (Fig. 4b–e). The binding energies of O 1 s at 530.5, 531.8 and 532.9 eV were associated with Bi-O binding, carbonate ions and adsorbed H₂O on the surface, respectively. For C 1s, three peaks at 285.0, 286.3 and 289.0 eV were observed. The binding energy at 285.0 eV was assigned to the CNFs, the peak at 286.3 eV ascribed to adventitious carbon species from the XPS measurement, and the peak at 289.0 eV was ascribed to carbonate ions in BOC. As shown in Fig. 4d, the two peaks of Bi 4f at 158.9 and 164.2 eV were assigned to Bi 4f_{7/2} and Bi 4f_{5/2}, while the two peaks of S 2p from MoS₂ at 162.6 and 163.8 eV corresponded to S 2p_{3/2} and S 2p_{1/2}. The binding energy of S 2s was also observed at 225.8 eV, and that of Mo⁴⁺ at 228.7 (Mo 3d_{5/2}) and 231.9 eV (Mo 3d_{3/2}). Surprisingly, Mo⁶⁺ and S⁶⁺ states were also detected, from which we infer that small amounts of surface oxide species were formed during the hydrothermal reaction [32,35]. The above analysis of the XPS spectra demonstrates the existence of BOC and MoS₂.

3.3. Optical properties

The optical properties of the as-prepared samples were investigated by UV-vis diffuse reflectance spectroscopy (DRS), as shown in Fig. 4f. The pure BOC microflowers exhibited an absorption edge at about 360 nm, and the intensity of their optical absorption was increased after they were modified onto the CNFs. Importantly, when MoS₂ was modified onto the surface of the above material, the visible-light absorption of the BOC-MoS₂-CNFs photocatalyst was further intensified, and its absorption edge was blue-shifted to 430 nm, suggesting that MoS₂ would enhance the performance of the photocatalyst under visible light.

The FT-IR spectra of the BOC, BOC-CNFs and BOC-MoS₂-CNFs are shown in Fig. S4 (Supporting Information). The characteristic bands of BOC were observed in the spectra of all three samples, demonstrating the existence of BOC microflowers. The absorption bands at 670 cm⁻¹ (in-plane deformation), 846 and 1730 cm⁻¹ (symmetric stretching mode), 1391 and 1468 cm⁻¹ (corresponding antisymmetric vibration) were indicative of CO₃²⁻ [33]. The absorption

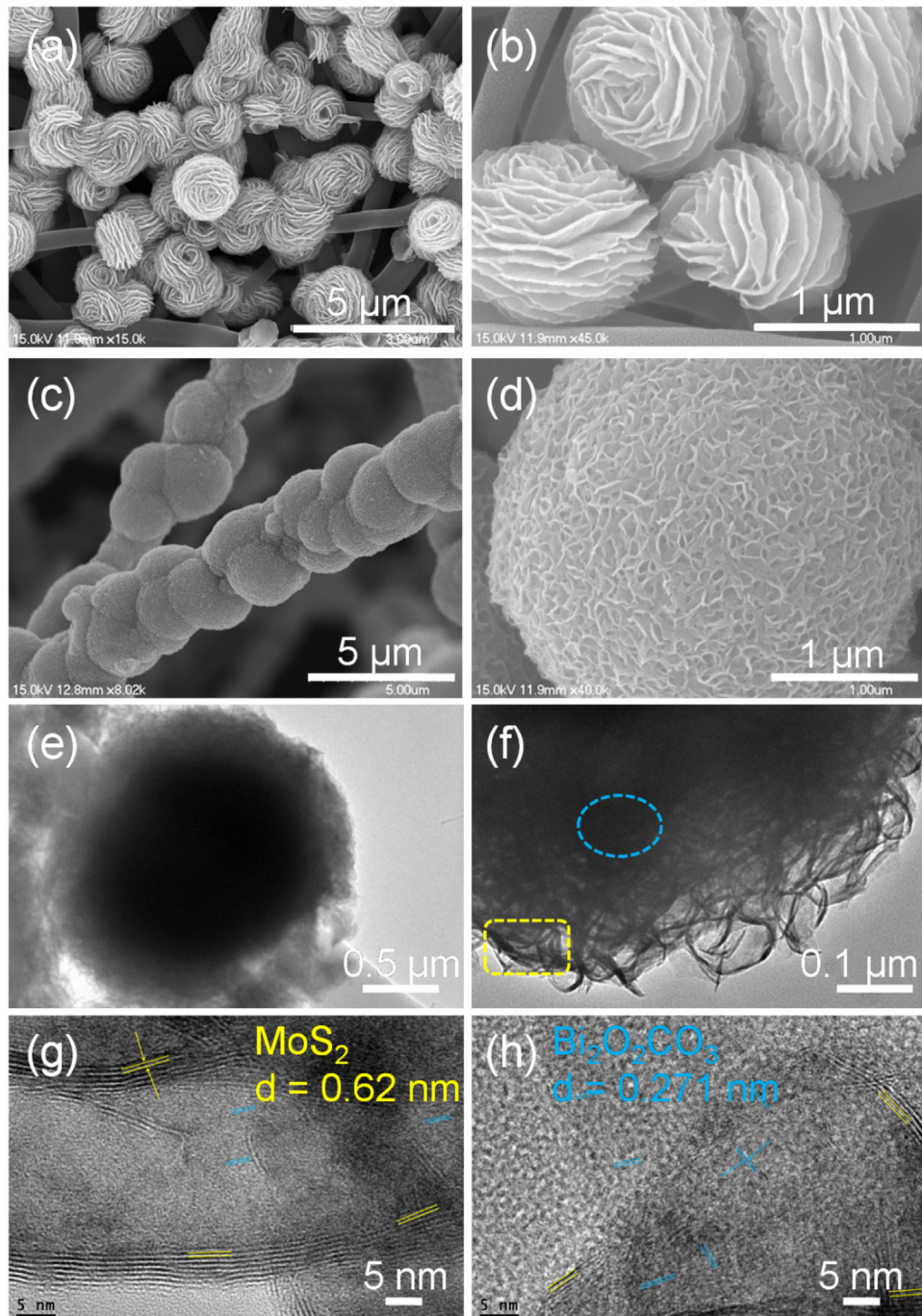


Fig. 1. SEM images of BOC-CNFs (a–b) and BOC-MoS₂-CNFs (c–d). TEM (e–f) and HRTEM images (g–h) of BOC-MoS₂-CNFs.

bands at 823, 1281 and 1560 cm^{−1} were assigned to the vibration of CNFs. Unfortunately, the vibration of MoS₂ was too weak to be clearly observed.

3.4. Electrochemical properties

The electrochemical behaviors of the as-obtained samples were investigated, as shown in Fig. 5. Photocurrent responses with good reproducibility were recorded upon excitation of BOC/ITO, BOC-CNFs/ITO and BOC-MoS₂-CNFs/ITO electrodes with visible-light irradiation (Fig. 5a). The responses were directly related to the electron transport and recombination efficiency of the photogenerated carriers. The photocurrent density of the BOC-CNFs was twice that

of pure BOC, which is consistent with the expected role of the CNFs in contributing to electron transport. Surprisingly, the BOC-MoS₂-CNFs exhibited a remarkably enhanced photocurrent density, from which can be inferred that MoS₂ benefitted the recombination of e[−]–h⁺. The chargetransfer resistance and separation efficiency of the charge carriers were further investigated by electrochemical impedance spectroscopy (EIS). As shown in Fig. 5b, the arc radius on the EIS Nyquist plot of BOC-MoS₂-CNFs was smaller than that of BOC and BOC-CNFs, indicating that the addition of MoS₂ substantially enhanced the separation and transfer efficiency of e[−]–h⁺ pairs, thereby improving the photocatalytic efficiency. Photoluminescence (PL) spectra are also used to investigate the separation or recombination of photogenerated electron-hole pairs of the pho-

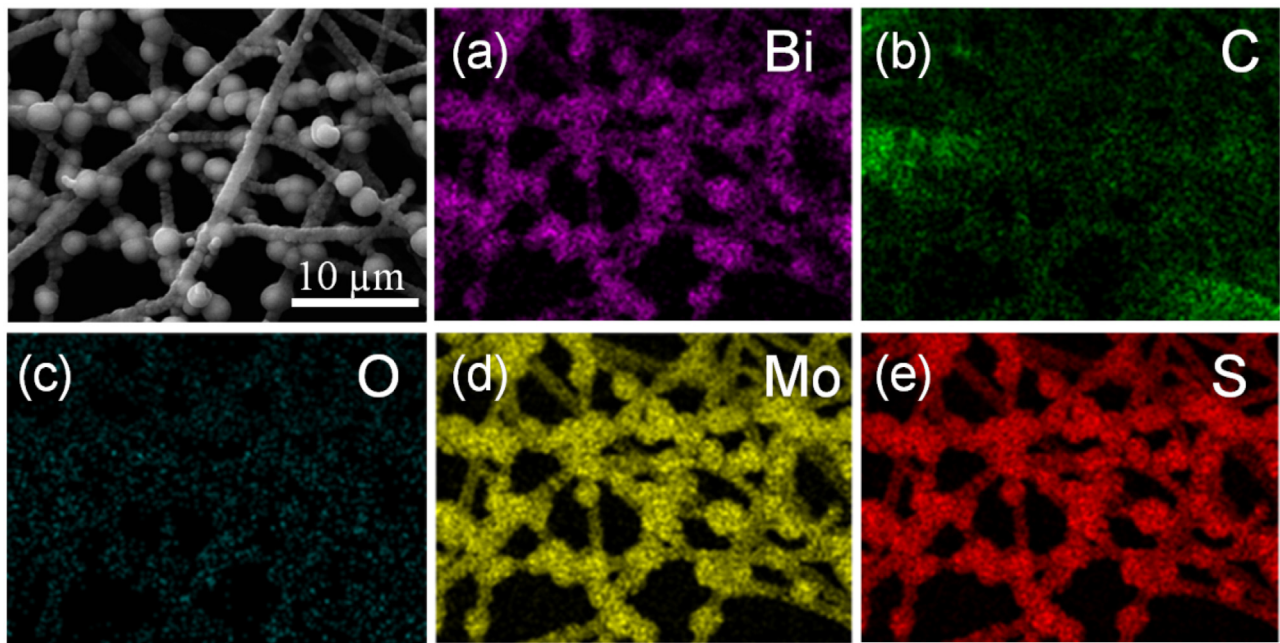


Fig. 2. SEM image of BOC-MoS₂-CNFs (top left) and EDS mapping images of Bi, C, O, Mo and S respectively (a-e).

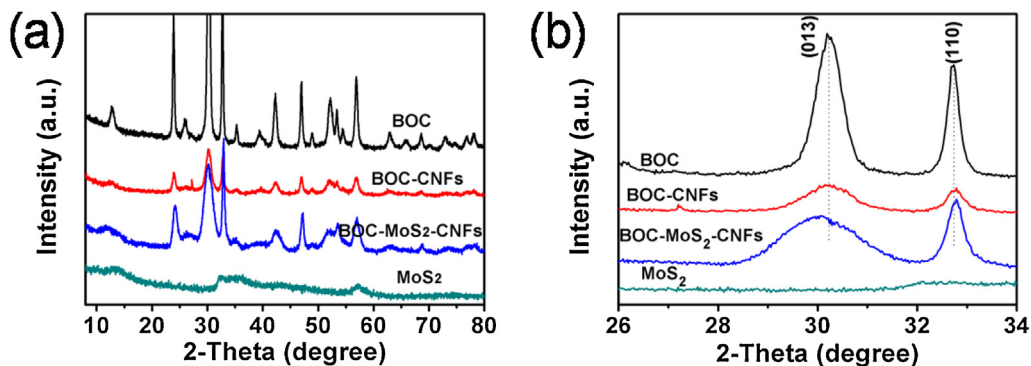


Fig. 3. XRD patterns (a) and enlarged view of the $2\theta = 26\text{--}35^\circ$ diffraction region (b) of the synthesized samples.

tocatalyst, as shown in Fig. S5 (Supporting Information). The PL intensity of BOC-MoS₂-CNFs is much lower than that of BOC-CNFs and BOC, and this result indicates that the nanocomposite photocatalyst BOC-MoS₂-CNFs has a strong ability of the separation and transfer of electrons and holes.

3.5. Photocatalytic performance for NO removal

The photocatalytic activity of the BOC-MoS₂-CNFs sample was evaluated for the degradation of NO at the indoor air level under visible irradiation to determine its capacity for air purification. We also compared its performance with pure BOC microflowers and the BOC-CNFs membrane. Fig. 6a shows the NO concentration (C/C_0) against irradiation time over CNFs, BOC, BOC-CNFs and BOC-MoS₂-CNFs under visible-light irradiation. Here, C_0 is the initial concentration of NO, and C is the concentration of NO after photocatalytic reaction for a length of time t . From Fig. 6a, it is evident that on pure CNFs, no photolysis of NO occurred even after irradiation for 30 min, confirming that CNFs have no intrinsic catalytic ability. With pure BOC microflowers, the NO removal ratio was only 32%, which is consistent with the previous report [32]. The poor photocatalytic ability of BOC is caused by various intrinsic properties of this material, for example, the fast recombination of $e^- - h^+$ pairs.

Encouragingly, BOC-CNFs exhibited higher photocatalytic activity, with an NO removal ratio of 43%. From this we deduced that the CNFs were conducive to electron transport and strongly inhibited the recombination of electron–hole $e^- - h^+$ pairs, thereby enhancing the activity of the photocatalyst. The introduction of MoS₂ makes BOC-MoS₂-CNFs photocatalyst displayed greater activity, and its ratio of NO removal attain to 68%. The photocatalyst effect of BOC-MoS₂-CNFs is higher than that of other Bi-based materials, such as the ratio of NO removal by Bi₂O₂CO₃-g-C₃N₄ is 35% [35], Bi self-doping Bi₂MoO₆ (Bi/Mo molar ratio is 2.05) is 55% [36], Bi₂WO₆-graphene is 60% [37] and BiOBr-graphene (Bi/graphene molar ratio is 50:1) is 40% [51]. In addition, the catalytic activity of photocatalyst which contains BOC was rapid: the NO concentrations were reduced almost to their final values within the first 5 min, remaining roughly constant thereafter. This demonstrated the high performance of the photocatalysts.

Based on previous literature, we propose a possible photocatalytic reaction mechanism, as shown in Scheme 2 [32,35]. As visible-active materials, BOC and MoS₂ can both be excited to produce $e^- - h^+$ pairs under visible-light irradiation. According to the conventional theory of double charge transfer, the photogenerated electrons of MoS₂ would transfer to the conduction band (CB) of BOC and the holes of BOC would migrate to the valence band (VB)

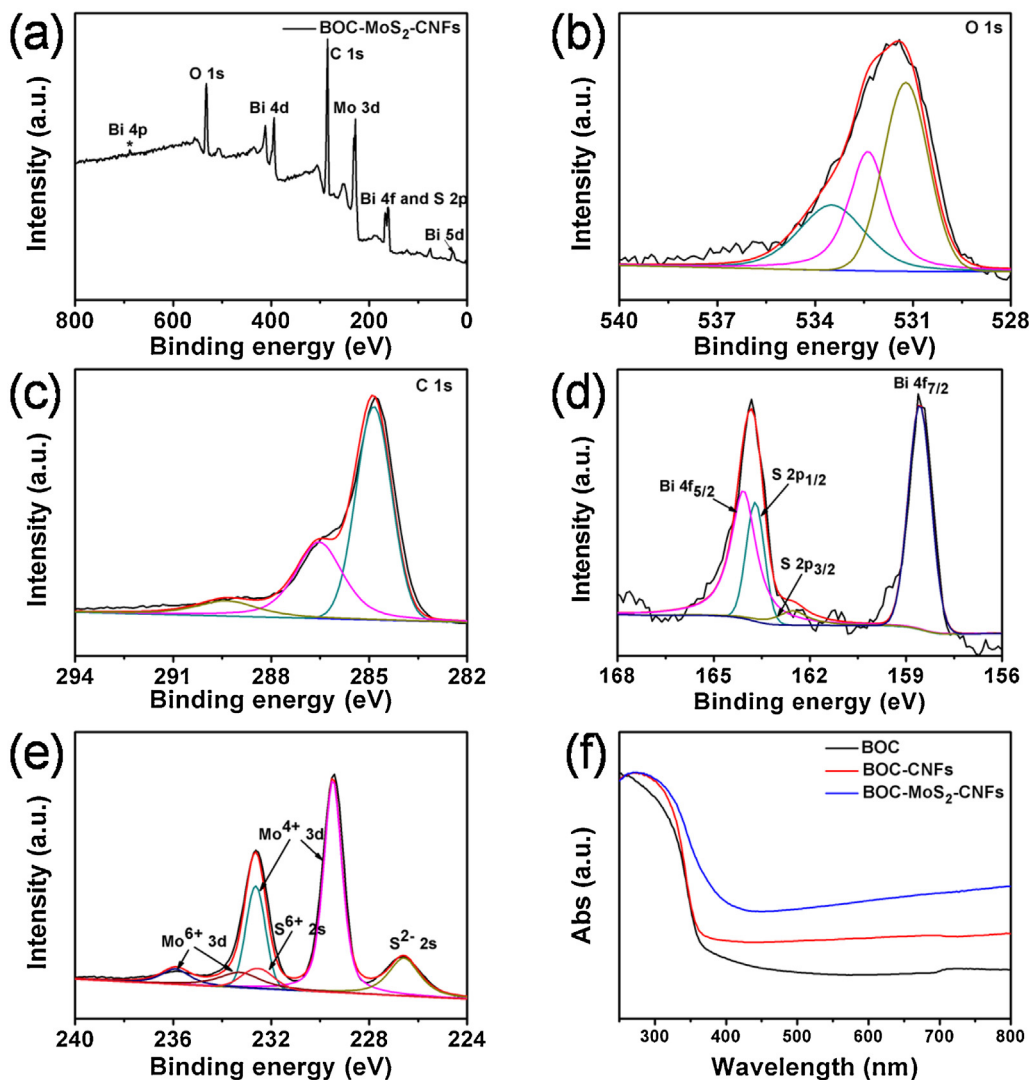


Fig. 4. XPS spectra of the BOC-MoS₂-CNFs sample (a) and high-resolution XPS spectra of O 1 s (b), C 1 s (c), Bi 4f and S 2p (d), Mo 3d and S 2s (e). UV-vis DRS absorption of as-prepared samples (f).

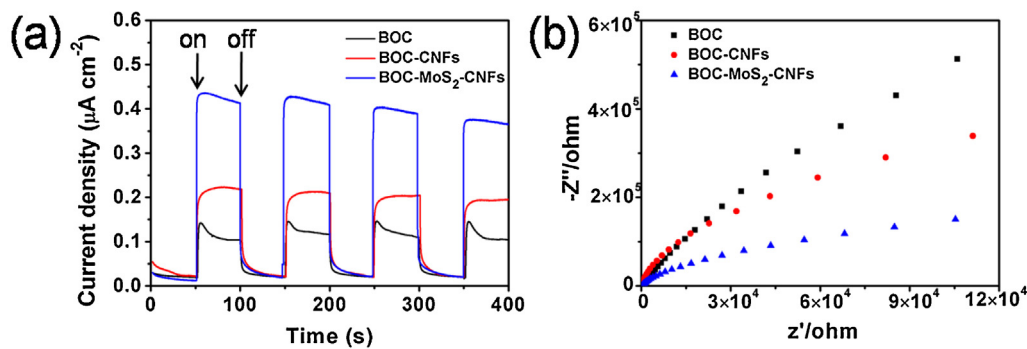


Fig. 5. Photocurrent transient (a) and electrochemical impedance spectra (b) of the as-obtained samples under visible-light irradiation.

of MoS₂, because the VB and CB potentials of BOC are both lower than those of MoS₂. However, we propose that in this photocatalytic reaction, the electrons in the CB of BOC and the holes in the VB of MoS₂ didn't follow a standard mechanism, as the CB potential of BOC is lower than the O₂/O₂⁻ redox couple and the oxidation ability of the h⁺ located in the VB of MoS₂ is not strong enough to directly oxidize NO. After careful research and analysis, we inferred

that the electrons in the VB of BOC were excited to the CB under visible-light irradiation, then easily transferred to the VB of MoS₂, where they recombined with its holes. Subsequently, the holes remaining in the VB of BOC, with strong oxidative power, could directly oxidize the NO in air to NO³⁻ (Eq 2). Meanwhile, the O₂ in air was reduced to •O₂⁻ (Eq 3), and the •O₂⁻ was further reduced to •OH (Eqs 4–5) to react with NO (Eq 6). Here, the produced e⁻–h⁺

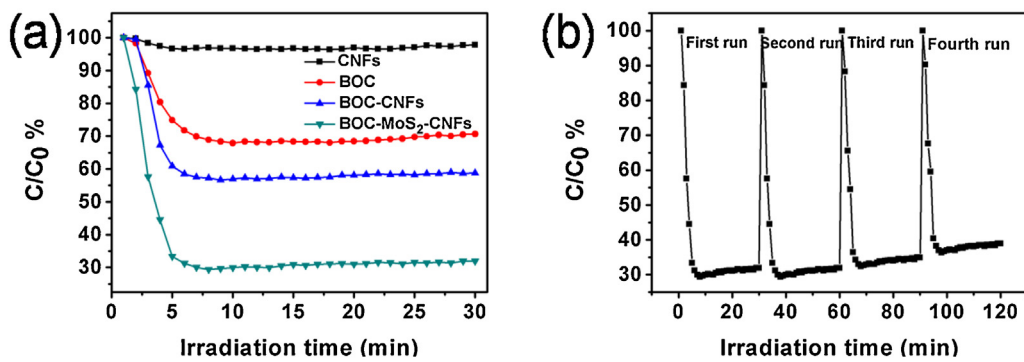
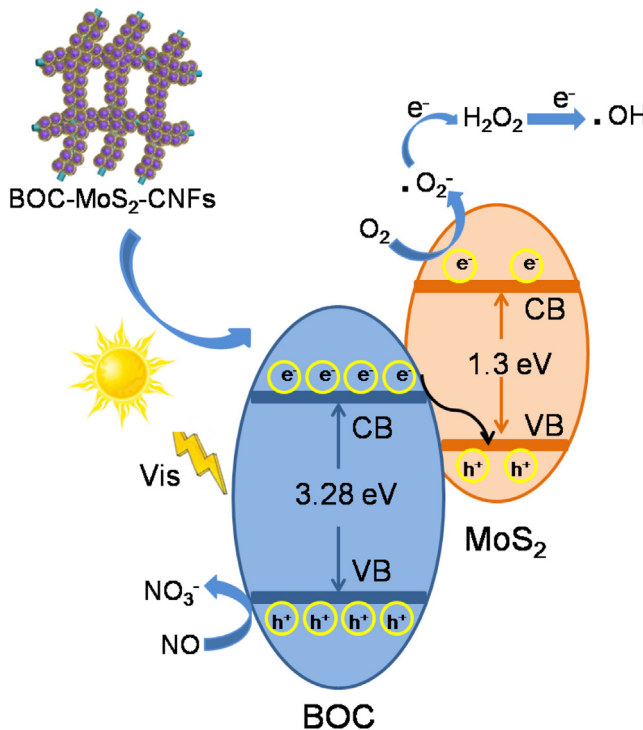
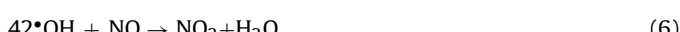
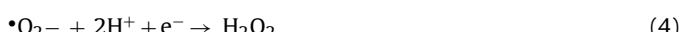
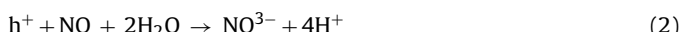
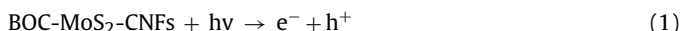


Fig. 6. Visible-light photocatalytic activities of CNFs, BOC, BOC-CNFs and BOC-MoS₂-CNFs samples for NO removal in air (a), and consecutive cycles of photocatalytic reactions for the photocatalytic degradation of NO (600 ppb) over BOC-MoS₂-CNFs under visible light (b).



Scheme 2. Photocatalytic mechanism of NO removal by BOC-MoS₂-CNFs.

pairs were separated sufficiently to prevent their recombination, and the migration rate of electrons was considerably enhanced by the action of the CNFs. Therefore, this mechanism (summarized in Eqs. (1–9)) enabled the BOC-MoS₂-CNFs photocatalysts to realize highly efficient removal of NO under visible-light irradiation.



To further confirm this mechanism, the electron spin resonance (ESR) spectroscopy were performed to detect the $\cdot\text{O}_2^-$ and $\cdot\text{OH}$, as shown in Fig. S6. The signals of the DMPO- $\cdot\text{O}_2^-$ species could be observed with dispersion of BOC-MoS₂-CNFs photocatalysts in methanol under visible light irradiation, as displayed in Fig. S6a. Additionally, four characteristic peaks with an intensity ratio of 1:2:2:1 were clearly observed for BOC-MoS₂-CNFs sample in aqueous dispersion systems (Fig. S6b), which testified to the production of $\cdot\text{OH}$ radicals. All these results are consistent with the mechanism we have proposed.

4.4. Photochemical and structural stability of photocatalyst

The recyclability and structural stability of photocatalysts are important for their potential applications. These factors were assessed for the photocatalyst BOC-MoS₂-CNFs by carrying out the photocatalytic removal of NO under visible-light irradiation for multiple runs. As shown in Fig. 6b, the NO removal ratio remained high after four consecutive runs, demonstrating that this photocatalysis photochemically stable and can be used repeatedly. More importantly, the photocatalyst can be easily recycled with tweezers and reused because of the introducing of CNFs. These properties demonstrate the potential suitability of BOC-MoS₂-CNFs for removing NO from the air.

5. Conclusion

In summary, BOC-MoS₂-CNFs nanocomposite photocatalysts were fabricated successfully by an efficient method. This photocatalyst exhibited excellent activity in removing NO at the parts per billion (ppb) level from air under visible-light irradiation. The NO removal ratio of 68% was higher than that of many other photocatalysts. The enhanced efficiency was not only attributed to the introduction of CNFs, which facilitated the transportation of electrons, but also to the MoS₂ nanosheets, which contributed to fast separation and transfer of electrons and holes. Cyclic testing of the photocatalytic process demonstrated that BOC-MoS₂-CNFs was stable and could be used repeatedly. The findings of this study demonstrate that BOC-MoS₂-CNFs membranes have a potential application value in the removal of NO from air in the future.

Acknowledgements

This work was supported by the Collaborative Innovation Center of Suzhou Nano Science and Technology. The authors gratefully acknowledge the financial support provided by the National Natural Science Foundation of China (21336005, 51573122), the Natural Science Foundation of Jiangsu Province (BK2012625), the National Key Technology R&D Program (2015BAC20B03-06) and the Sci-

ence and Technology Program for Social Development of Jiangsu (BE2015637).

Appendix A. Supplementary data

Supplementary data associated with this article can be found, in the online version, at <http://dx.doi.org/10.1016/j.apcatb.2017.05.088>.

References

- [1] R.-J. Huang, Y. Zhang, C. Bozzetti, K.-F. Ho, J.-J. Cao, Y. Han, K.R. Daellenbach, J.G. Slowik, S.M. Platt, F. Canonaco, *Nature* 514 (2014) 218–222.
- [2] Y. Sun, G. Zhuang, A. Tang, Y. Wang, Z. An, *Environ. Sci. Technol.* 40 (2006) 3148–3155.
- [3] M. Elser, R.-J. Huang, R. Wolf, et al., *Atmos. Chem. Phys.* 16 (2016) 3207–3225.
- [4] K.-F. Ho, S.S.H. Ho, R.-J. Huang, H.-C. Chuang, et al., *Atmos. Environ.* 126 (2016) 162–170.
- [5] R.J. Gorte, J.L. Gland, *Surf. Sci.* 102 (1981) 348–358.
- [6] B. Xiao, P.S. Wheatley, X. Zhao, A.J. Fletcher, S. Fox, A.G. Rossi, I.L. Megson, A. Bordiga, L. Regli, K.M. Thomas, R.E. Morris, *J. Am. Chem. Soc.* 129 (2007) 1203–1209.
- [7] C.E. Brown, P.G. Hall, *J. Colloid. Interface. Sci.* 42 (1973) 334–341.
- [8] Y.B. Davidova, E.D. Schroeder, D.P.Y. Chang, *SciTech. Connect.* (1997) 18–22.
- [9] M. Noris, M. Todeschini, F. Casiraghi, D. Roccatello, G. Martina, L. Imberti, F. Gaspari, M. Atti, G. Remuzzi, *Am. J. Kidney. Dis.* 32 (1998) 115–124.
- [10] J.M. Barnes, W.A. Apel, K.B. Barrett, *J. Hazard. Mater.* 41 (1995) 315–326.
- [11] Z. Lian, F. Liu, H. He, X. Shi, J. Mo, Z. Wu, *Chem. Eng. J.* 250 (2014) 390–398.
- [12] H. Xu, Y. Wang, Y. Cao, Z. Fang, T. Lin, M. Gong, Y. Chen, *Chem. Eng. J.* 240 (2014) 62–73.
- [13] Z. Liu, J. Zhu, J. Li, L. Ma, S.I. Woo, *ACS Appl. Mater. Interfaces.* 6 (2014) 14500–14508.
- [14] A. Boubnov, H.W.P. Carvalho, D.E. Doronkin, et al., *J. Am. Chem. Soc.* 136 (2014) 13006–13015.
- [15] U. Deka, I. Lezcano-Gonzalez, B.M. Weckhuysen, A.M. Beale, *ACS Catal.* 3 (2013) 413–427.
- [16] Q. Zhang, Y. Zhou, F. Wang, F. Dong, W. Li, H. Li, G.R. Patzke, *J. Mater. Chem. A.* 2 (2014) 11065–11072.
- [17] Q. Zhang, Y. Huang, S. Peng, Y. Zhang, et al., *Appl. Catal. B: Environ.* 204 (2017) 346–357.
- [18] A. Trapalis, N. Todorova, T. Gianakopoulou, N. Boukos, T. Speliotis, D. Dimotikali, J. Yu, *Appl. Catal. B: Environ.* 180 (2016) 637–647.
- [19] K. Fujiwara, S. Pratsinis, A. I. Ch. E. 63 (2017) 139–146.
- [20] M.-Z. Guo, T.-C. Ling, C.-S. Poon, *Cem. Concr. Comp.* 36 (2013) 101–108.
- [21] L. Chen, Z. Si, X. Wu, D. Weng, *ACS Appl. Mater. Interfaces.* 6 (2014) 8134–8145.
- [22] S. Xiao, W. Zhu, P. Liu, F. Liu, W. Dai, D. Zhang, W. Chen, H. Li, *Nanoscale.* 8 (2016) 2899–2907.
- [23] D. Uner, I. Bayar, T. Tabari, *Appl. Surf. Sci.* 354 (2015) 260–266.
- [24] J. Ma, H. Wu, Y. Liu, H. He, *J. Phys. Chem. C.* 118 (2014) 7434–7441.
- [25] M.-Z. Guo, C.-S. Poon, *Build. Environ.* 70 (2013) 102–109.
- [26] S. Yang, Y. Fu, Y. Liao, S. Xiong, Z. Qu, N. Yan, J. Li, *Catal. Sci. Technol.* 4 (2014) 224–232.
- [27] F. Dong, Z. Zhao, T. Xiong, Z. Ni, W. Zhang, Y. Sun, W.-K. Ho, *ACS Appl. Mater. Interfaces.* 5 (2013) 11392–11401.
- [28] G. Dong, L. Yang, F. Wang, L. Zang, C. Wang, *ACS. Catal.* 6 (2016) 6511–6519.
- [29] Y. Sun, T. Xiong, Z. Ni, J. Liu, F. Dong, W. Zhang, W.-K. Ho, *Appl. Surf. Sci.* 358 (2015) 356–362.
- [30] T. Sano, S. Tsutsui, K. Koike, T. Hirakawa, Y. Teramoto, N. Negishi, K. Takeuchi, *J. Mater. Chem. A* 1 (2013) 6489–6496.
- [31] P. Li, W. Zhang, Y. Zhang, Y. Sun, F. Dong, *RSC Adv.* 6 (2016) 96334–96338.
- [32] T. Xiong, M. Wen, F. Dong, J. Yu, et al., *Appl. Catal. B: Environ.* 199 (2016) 87–95.
- [33] F. Dong, W.-K. Ho, S.C. Lee, Z. Wu, M. Fu, S. Zou, Y. Huang, *J. Mater. Chem.* 21 (2011) 12428–12436.
- [34] Y. Huang, W. Wang, Q. Zhang, J.-J. Cao, R.-J. Huang, W. Ho, S.C. Lee, *Sci. Rep.* 6 (2016) 1–9.
- [35] Z. Wang, Y. Huang, W. Ho, J. Cao, Z. Shen, S.C. Lee, *Appl. Catal. B: Environ.* 199 (2016) 123–133.
- [36] X. Ding, W. Ho, J. Shang, L. Zhang, *Appl. Catal. B: Environ.* 182 (2016) 316–325.
- [37] Y. Zhou, X. Zhang, Q. Zhang, F. Dong, F. Wang, Z. Xiong, *J. Mater. Chem. A* 2 (2014) 16623–16631.
- [38] G. Dong, W. Ho, L. Zhang, *Appl. Catal. B: Environ.* 168–169 (2015) 490–496.
- [39] R. Sugranez, J. Balbuena, M. Cruz-Yusta, F. Martin, J. Morales, L. Sanchez, *Appl. Catal. B: Environ.* 165 (2015) 529–536.
- [40] M.-V. Sofianou, M. Tassi, V. Psycharis, et al., *Appl. Catal. B: Environ.* 162 (2015) 27–33.
- [41] D. Zheng, C. Pang, Y. Liu, X. Wang, *Chem. Commun.* 51 (2015) 9706–9709.
- [42] F. Dong, S.C. Lee, Z. Wu, Y. Huang, M. Fu, W.-K. Ho, S. Zou, B. Wang, *J. Hazard. Mater.* 195 (2011) 346–354.
- [43] X. Feng, W. Zhang, H. Deng, Z. Ni, F. Dong, Y. Zhang, *J. Hazard. Mater.* 322 (2017) 223–232.
- [44] Y. Zhang, D. Li, Y. Zhang, X. Zhou, S. Guo, L. Yang, *J. Mater. Chem. A* 2 (2014) 8273–8280.
- [45] Y. Zhong, X. Qiu, D. Chen, N. Li, Q. Xu, H. Li, J. He, J. Lu, *ACS Appl. Mater. Interfaces.* 8 (2016) 28671–28677.
- [46] H. Wu, D. Chen, N. Li, Q. Xu, H. Li, J. He, J. Lu, *Nanoscale.* 8 (2016) 12066–12072.
- [47] C. Zhao, J. Kong, X. Yao, X. Tang, Y. Dong, S.L. Phua, X. Lu, *ACS Appl. Mater. Interfaces.* 6 (2014) 6392–6398.
- [48] D. Zheng, G. Zhang, X. Wang, *Appl. Catal. B: Environ.* 179 (2015) 479–488.
- [49] G. Zhang, M. Zhang, X. Ye, X. Qiu, S. Lin, X. Wang, *Adv. Mater.* 26 (2014) 805–809.
- [50] D. Zheng, C. Pang, Y. Liu, X. Wang, *Chem. Commun.* 51 (2015) 9706–9709.
- [51] Z. Ai, W. Ho, S. Lee, *J. Phys. Chem. C.* 115 (2011) 25330–25337.